



*National Institute
for Petroleum
and Energy
Research
Post Office Box 2565
Bartlesville, OK 74005*

Status Report

**GEOLOGICAL INTERPRETATION OF NEAR-OUTCROP
GROUND-PENETRATING RADAR SURVEY OF THE
ALMOND FORMATION, OUTCROP G,
TIDAL SANDSTONES**

for

**Management and Operating Contract
for the Department of Energy's
National Oil and Related Programs**

by

Douglas A Lawson, Consultant
and
Richard A. Schatzinger
BDM Petroleum Technologies
Under Contract to
BDM-Oklahoma, Inc.

May 1998

Work Performed Under Contract No.
DE-AC22-94PC91008

Prepared for
U.S. Department of Energy
National Petroleum Technology Office

**GEOLOGICAL INTERPRETATION OF NEAR-OUTCROP
GROUND-PENETRATING RADAR SURVEY OF THE
ALMOND FORMATION, OUTCROP G,
TIDAL SANDSTONES**

for

**Management and Operating Contract
for the Department of Energy's
National Oil and Related Programs**

Work Performed Under Contract No.
DE-AC22-94PC91008

Prepared for
U.S. Department of Energy
National Petroleum Technology Office

DISCLAIMER

This report was prepared as an account of work sponsored by an agency of the United States Government. Neither the United States Government nor any agency thereof, nor any of their employees, makes any warranty, expressed or implied, or assumes any legal liability or responsibility for the accuracy, completeness, or usefulness of any information, apparatus, product, or process disclosed, or represents that its use would not infringe privately owned rights. Reference herein to any specific commercial product, process, or service by trade name, trademark, manufacturer, or otherwise does not necessarily constitute or imply its endorsement, recommendation, or favoring by the United States Government or any agency thereof. The views and opinions of authors expressed herein do not necessarily state or reflect those of the United States Government or any agency thereof.

BDM-Oklahoma, Inc.
P.O. Box 2565
Bartlesville, Oklahoma 74005

ABSTRACT

The data from a radar survey over the sandstones at outcrop G of the Almond formation provide an opportunity to determine the effectiveness of ground-penetrating radar in mapping interwell rock-body geometry of a tidal sequence. This survey was designed to determine the limits of ground-penetrating radar both in the conductivity of the rock mass, the spacing of survey lines and transmitter-receiver pair, and frequency of the signal. Four strike lines were surveyed, including their extensions, multiple frequency duplicates, and common midpoint equivalence. Eight dip lines, including their extensions, were shot starting from the tidal channel strike line at 195 ft, 315 ft, 415 ft, 635 ft, 855 ft, and 1075 ft from the x-y origin of the geological survey.

The quality of the data was strongly affected by the high water saturation of the outcrop. This caused strong coupling between the antennae and marked attenuation of the signal.

The best lines for stratigraphic interpretation are the tidal delta common midpoint line, the portion of the dip line at 1075 ft, and the 100 MHz and 50 MHz oyster marker bed lines. In the tidal delta line and the intersecting dip 1075 line, most of the events terminate against each other, giving the section a large cross-bedded appearance. The lower portion of the oyster marker bed line exhibits the alternating sandstone and shale/coal bedding seen in the Almond formation outcrop G and core hole No. 2. These data demonstrate that a closely spaced ground-penetrating radar grid over the tidal delta sandstone would generate data for a 3D permeability image. They also show that only under the driest conditions could an interwell scale survey succeed.

The velocity of propagation through the tidal delta sandstone of 0.21 ft/ns (0.07m/ns) was calculated using the time difference of the same event among offset traces. This velocity was used to make a general linear conversion of time to depth.

In a sequence of sandstones and shales such as the Almond formation at outcrop G, a preliminary electrical survey is essential to determine when conditions are suitable for a ground-penetrating radar survey. For further quality assurance, standard seismic interpretation software should be used during data acquisition so the survey design can be adjusted to suit the field conditions.

Table of Contents

1.0	INTRODUCTION.....	1
2.0	PRELIMINARY EXAMINATION	7
3.0	IMPROVING THE RADAR IMAGE.....	8
4.0	STRATIGRAPHIC INTERPRETATION.....	10
5.0	VELOCITY ANALYSIS.....	14
6.0	CONCLUSIONS.....	15
7.0	REFERENCES.....	16
	APPENDIX.....	19

List of Tables

1	Dip lines*.....	6
2	Strike lines (number in name indicates signal frequency).....	7
3	Common midpoint (3-fold) strike line.....	7

List of Figures

1	Stratigraphic column for outcropping Upper Cretaceous units in the study area.....	3
2	Location map of the study area on the eastern flank of the Rock Springs uplift, southwestern Wyoming.....	3
3	Outcrop stratigraphic cross section is nearly parallel to depositional strike. Note the breaks in tidal channel facies and the complexity of tidal inlet fill that can be found between distances much less than that of 40-acre well spacing.....	4
4	Location of the GPR survey lines at outcrop G.....	5
5	Dip line at 855 ft without any processing.....	8

6	Distortion of signal due to DC coupling in line tdchn2s (MHz).....	9
7	Shots of varying offset showing degree of DC coupling.....	9
8	Tidal delta sandstone. Automatic gain control with a 60 ns window	10
9	Stratigraphic interpretation of tidal delta GPR profile shown in Figure 8.....	11
10	Dip line at 1075 ft with automatic gain control with a 60 ns window.....	11
11	Stratigraphic interpretation of the tidal delta sandstone dip line 1075 ft shown in Figure 10.....	12
12	Strike line on oyster marker bed	13
14	Velocity analysis of common midpoint traces centered on tdcmp line trace 72 for ground wave arrival.....	15
A1	Dip line at 415 ft without any processing.....	19
A2	Dip line at 1075 ft. Automatic gain control applied with 60 ns window	19
A3	Strike line on oyster marker bed. Automatic gain control applied with 60 ns window ...	20
A4	Middle shoreface strike line from 195 ft to 555 ft. Automatic gain control applied with 60 ns window	20
A5	Continuation of middle shoreface strike line from 561 ft to 741 ft. Automatic gain control applied with 60 ns window	20
A6	Middle shoreface strike line from 951 ft to 1077 ft. Automatic gain control applied with 60 ns window	21

GEOLOGICAL INTERPRETATION OF NEAR-OUTCROP GROUND-PENETRATING RADAR SURVEY OF THE ALMOND FORMATION, OUTCROP G, TIDAL SANDSTONES

1.0 INTRODUCTION

Outcrop studies (e.g., Misra, Cil, Schatzinger, and Wheeler 1997; Schatzinger and Tomutsa 1997; Schatzinger and Wheeler 1997) provide reservoir rock architectural information from within the spacing of wells. Photographic analysis of surface exposure has been the primary source of detailed information about the geometry and internal structure of outcropping reservoir rock bodies. However, the derivation of rock geometry and internal bounding surfaces from outcrop photographs is hampered by optical distortion, varying angles of view, shadows, and most important, incomplete exposures of the rock face. Relating the outcrop photography to flow properties is inhibited by a confounded relation between rock color and petrophysical properties.

This survey was designed to determine the limits of ground-penetrating radar (GPR) in the conductivity of the rock mass, the spacing of survey lines and transmitter-receiver pair, and frequency of the signal. There are many potential benefits associated with this kind of survey. Near-outcrop GPR surveys do not exhibit any of the weaknesses mentioned above for the photographic method. The radar signal responds to contrasts in electrical conductivity which can be related to fluid transmissivity just as Ohm's Law can be related to Darcy's Law.

However, the attenuation of the signal by conductive clays within a sequence of interbedded terrigenous clastics must be evaluated. The data from survey over the sandstones at outcrop G of the Almond formation provide an opportunity to determine the effectiveness of GPR in mapping interwell rock-body geometry of a tidal sequence.

Near-outcrop GPR surveys over distances equivalent to less than a five-acre spacing have been made over carbonate rocks (Liner and Liner 1995) and fluvial sandstones (McMechan et al. 1997). These surveys not only were over extremely short distance but also were conducted on

the most favorable conditions. The carbonate and chert section contained no significant shale, thus providing an extremely low conductivity rock mass to probe. The Utah survey (McMechan et al. 1997) was confined to within a single, relatively clay-free fluvial channel sandstone. In addition to the favorable rock conductivity, the Ferron sandstone has little likelihood of perched groundwater within the sandstones because the surrounding edges of the butte allow immediate drainage.

In recent years GPR has been used to solve many aspects of detailed stratigraphic analysis when penetration depths of no more than about 30 m was required. Specific examples include mapping bedrock depth (Annan and Vaughan 1982), fracture detection in bedrock (Davis and Annan 1986), the location of old mine stopes (Annan 1988), and imaging continuous reflection from the water table at depths of 5–11 ft below the land surface.

Radar profiles have proven useful in determining architectural element geometry in both consolidated and poorly consolidated to unconsolidated sediments. Jol and Smith (1991) found GPR techniques useful in areas of limited subsurface control in six Canadian lacustrine deltas. The radar information was found to provide a perspective of deltaic architecture that would otherwise only be available in laterally continuous, extensive exposures. Success in imaging was limited in silt and clays, but results from sand and gravel deposits revealed detailed facies assemblages. Other GPR studies in poorly consolidated sediments include determination of 3D geometry of glacial outwash plain deposits in Denmark (Olsen and Andreasen 1995); assessment of coastal barrier sand volumes in Maine (Van Heteren, FitzGerald, Barber, Kelley, and Belknap 1996) where radar penetration of 8–10 meters was accomplished; and recognition of eight reflection configurations of “radar facies” that can be used to characterize mid- to high-latitude coastal environments (Van Heteren, FitzGerald, McKinlay, and Buynevich 1998).

Recent examples of GPR studies in consolidated sediments include that of Stephens (1994), who found that radar was an effective means of delineating subsurface stratigraphy in the Kayenta formation, southwestern Colorado. Stephens reported that GPR “plusses” include high resolution, easy mobility, and rapid rate of data collection; drawbacks include shallow penetration (typically less than 15 m) and limitation to low-conductivity environments. GPR profiling also was conducted in Triassic alluvial sandstones in southern Germany. Aigner, Aspiron, Hornung, Junghat, and Kostrewa (1996) used an integrated approach to characterizing the Upper Triassic Keuper sandstones that incorporated sequence stratigraphy of facies, architectural element identification of sedimentary cycles aided by GPR profiling and petrophysical measurements.

The Almond formation outcrop (Figs. 1 and 2), which lies on the southeastern rim of the Rock Springs uplift, referred to as outcrop G by Roehler (1988), consists of repeating cycles of tidal sands, marsh shales, and coals. A detailed stratigraphic and depositional interpretation has been provided by Schatzinger (Schatzinger et al. 1993; Cheng et al. 1994). The stratigraphic cross-sectional interpretation of outcrop G based on measured geological sections, gamma ray profiles, and photomosaic analysis is presented in Figure 3.

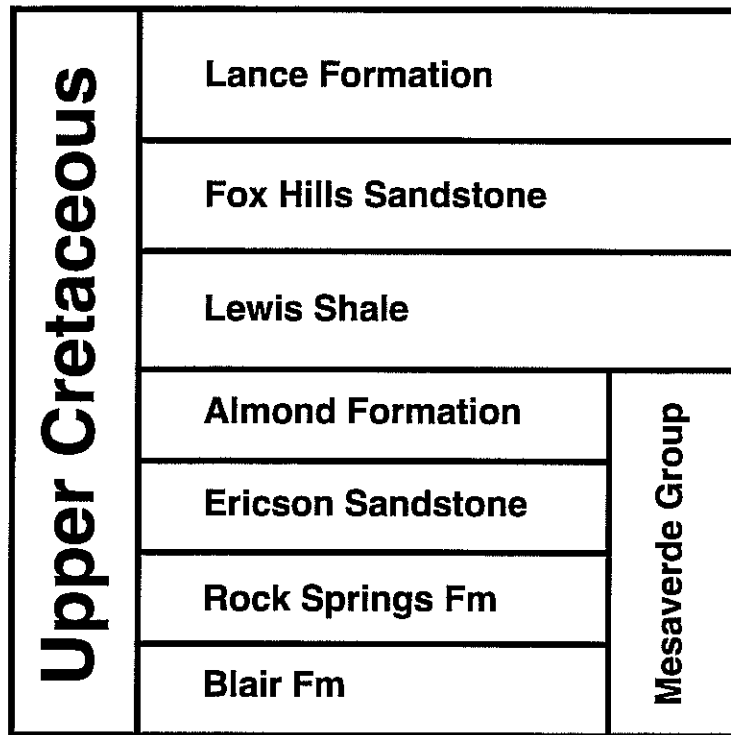


Figure 1 Stratigraphic column for outcropping Upper Cretaceous units in the study area

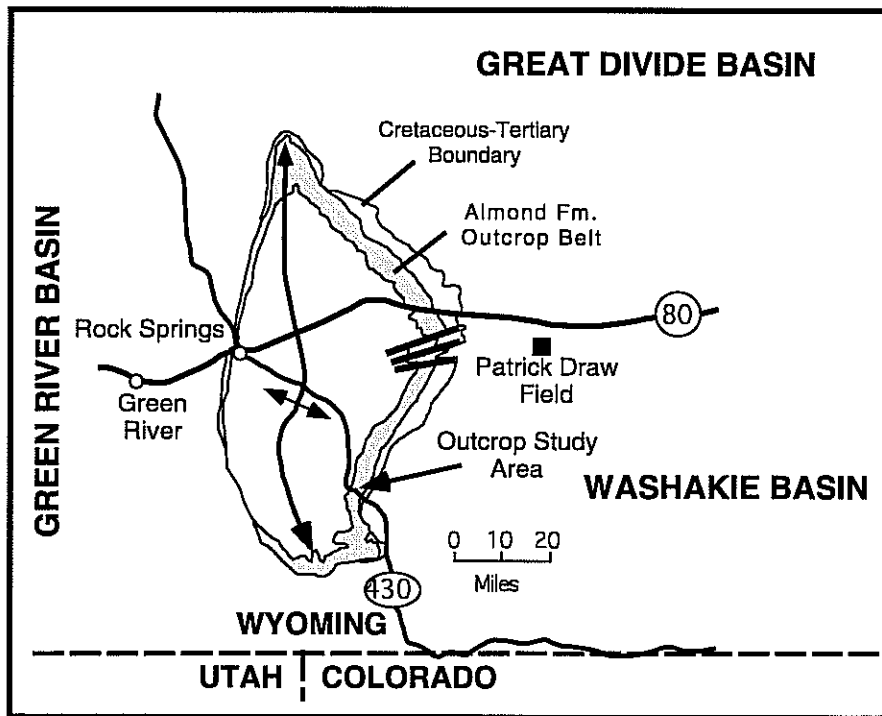


Figure 2 Location map of the study area on the eastern flank of the Rock Springs uplift, southwestern Wyoming

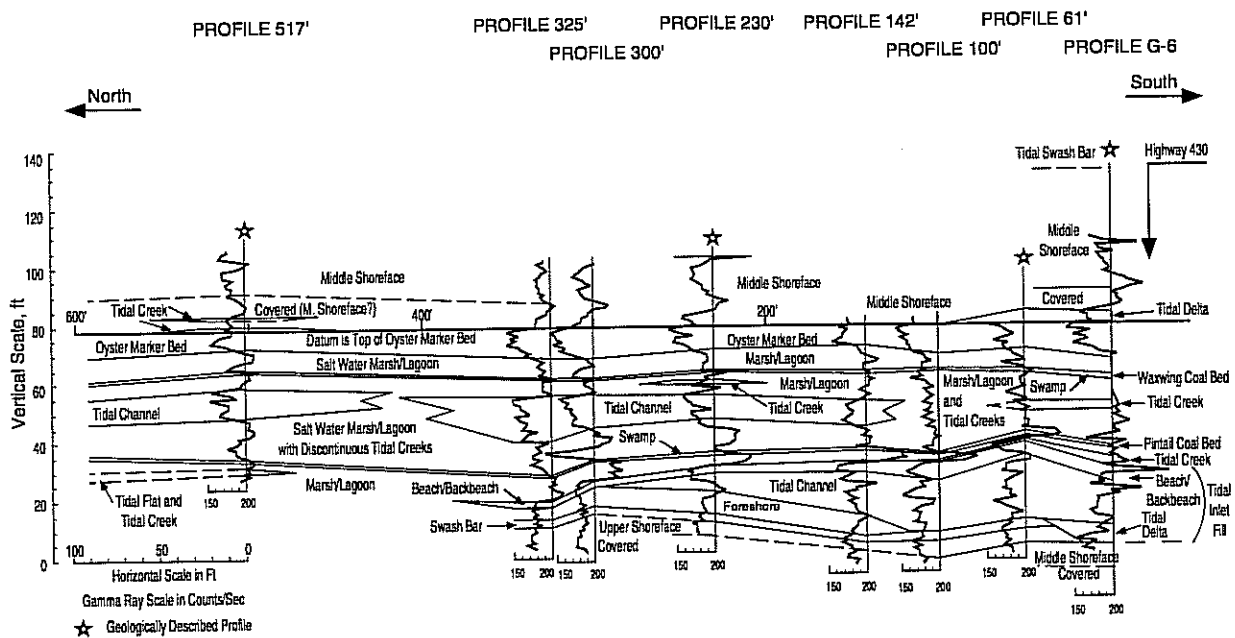


Figure 3 Outcrop stratigraphic cross section is nearly parallel to depositional strike. Note the breaks in tidal channel facies and the complexity of tidal inlet fill that can be found between distances much less than that of 40-acre well spacing.

From bottom to top, the depositional sequence of outcrop G consists of:

- Middle shoreface sandstone
- Upper shoreface and beach sandstone
- Tidal inlet sandstone
- Marsh and swamp coal and shale
- Tidal channel sandstones
- Marsh and lagoon shale
- Oyster bed and middle shoreface sandstones (mostly covered)
- Tidal delta sandstone
- Marsh and lagoon shale with discontinuous tidal creek siltstone
- Shelf sandstone and muds (mostly covered)

The tidal channel sandstones are generally 8 ft thick and extend laterally about 240 ft. The shoreface/beach sandstones are about 10 ft thick and extend over 325 ft laterally. The oyster bed (4 ft thick) and tidal delta (10 ft thick) sandstones extend for more than 500 ft. The interbeds of shale are from 8–15 ft thick. The entire section from the shoreface sandstone at the base of the outcrop to the top of the tidal delta sandstone is about 130 ft thick.

Because of the geometry of the outcrop and exposed sandstones, the survey (Fig. 4) was designed to test the radar's ability to image the sequence of sediments. It consisted of a grid of dip lines separated by 220 ft and perpendicular strike lines running along the tops of the outcropping sandstones. The two antennae were separated by 6 ft unless stated otherwise. The frequency of the pulse was 50 MHz, except where stated. The sampling rate was generally greater than one sample per 800 picoseconds (ps).

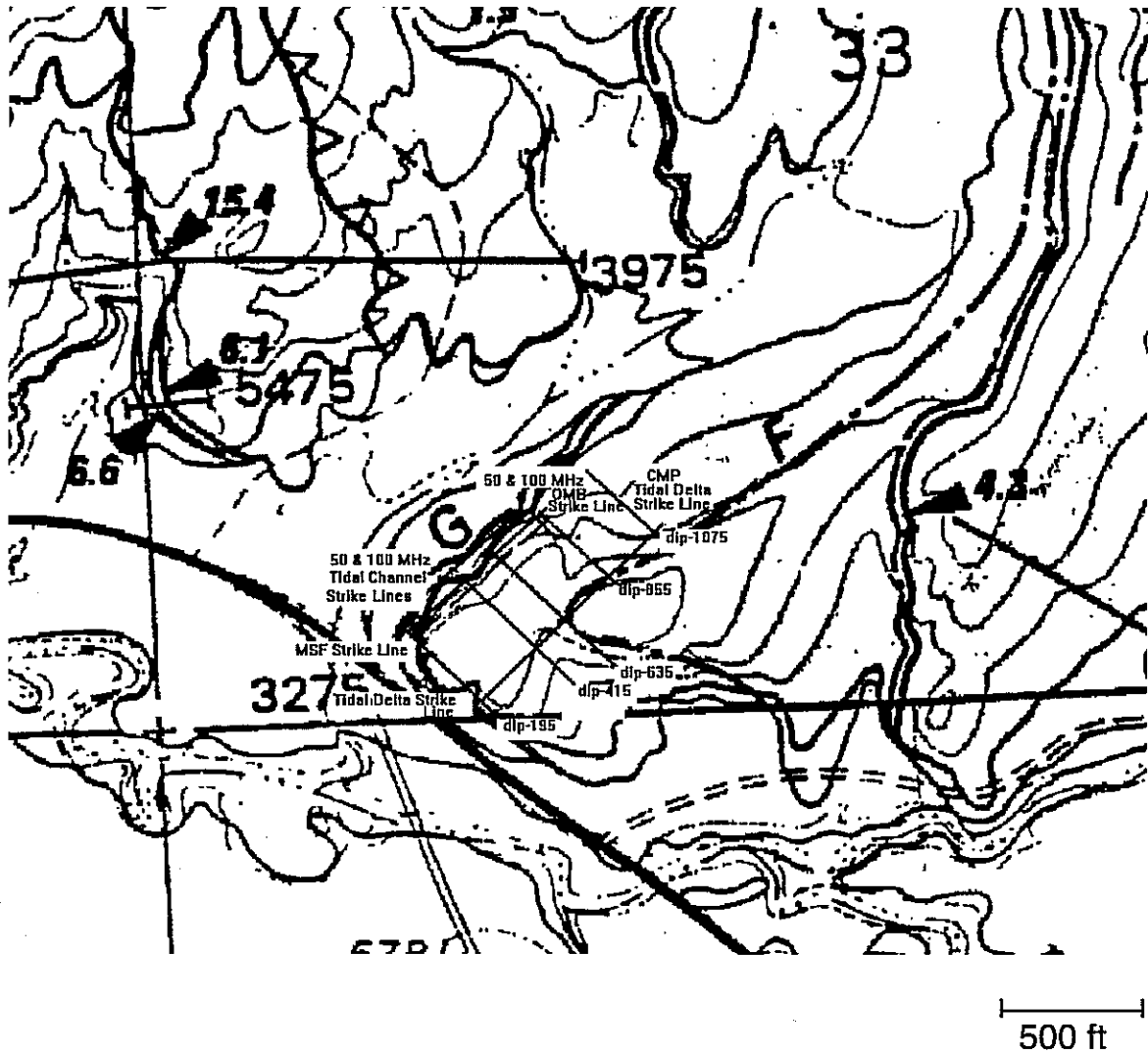


Figure 4 Location of the GPR survey lines at outcrop G

Eight dip lines, including their extensions (Table 1) were shot starting from the Tidal Channel strike line at 195 ft, 315 ft, 415 ft, 635 ft, 855 ft, and 1075 ft from the x-y origin of the geological survey (see Chang et al. 1995). These lines were shot on shaly terrain and exhibit no meaningful events except where crossing exposed sandstones. It is where these lines cross the strike lines shot along the top of exposed sandstones that their usefulness is demonstrated. Cross-ties of stratigraphic events at these intersections are helped in evaluating the usefulness of GPR for generating interwell scale 3D stochastic simulations and fluid flow models.

Table 1 Dip lines*

Line Name	Date	Number of Traces	Length, ft	Starting & Ending Coordinates
Dip 195	06/17/96	60	354 ft	0 - 354
Dip 195x	06/17/95	17	96 ft	354 - 450
Dip 315x	06/17/95	12	66 ft	0 - 66
Dip 415	06/16/95	59	348 ft	0 - 348
Dip 415x	06/16/95	21	120 ft	348 - 468
Dip 635	06/16/95	72	426 ft	0 - 426
Dip 855	06/17/95	58	342 ft	0 - 342
Dip 1075	06/19/95	41	240 ft	0 - 240
Dip 1075x	06/19/95	43	252 ft	240 - 492

* Number indicates x-coordinate position

Four strike lines were surveyed, including their extensions, multiple frequency duplicates and common midpoint equivalence (Table 2). These include, in increasing stratigraphic order, the middle shoreface, tidal channel, oyster marker-bed, and tidal delta sandstones. These sections generally exhibit some stratigraphically meaningful events. However, the quality of these survey lines was greatly affected by near-surface groundwater.

The line named tdcmp (Table 3) was composed from the third trace of the 50-MHz common-midpoint survey. This was done to avoid the distortion in the signal seen in the more closely spaced shots which thereby facilitated a stratigraphic interpretation of the tidal delta strike line.

Table 2 Strike lines (number in name indicates signal frequency)

Line Name	Date	Number of Traces	Length, ft	Starting & Ending Coordinates
omb 100*	06/14/95	10	54 ft	315 - 368
omb 50	06/14/95	7	36 ft	315 - 350
strmsfn** at 185	06/21/95	92	546 ft	195 - 741
strmsfnx	06/21/95	22	126 ft	951 - 1077
strobsexb	06/21/95	43	252 ft	315 - 63
strombsw	06/20/95	37	216 ft	615 - 399
strombsx	06/20/95	19	108 ft	425 - 317
strtdn ^f	06/20/95	32	186 ft	315 - 501
strtdnxa	06/20/95	10	54 ft	1027 - 1441
strtdnxb	06/20/95	2	6 ft	1225 - 1231
strtdnxz	20/06/95	62	366 ft	1075 - 1441
tdchn1nx ^{ff} 100	06/21/95	42	61.5 ft	605 - 666.5
tdchn1nx50	06/21/95	42	61.5 ft	605 - 666.5
tdchn1-100	06/18/95	61	90 ft	0 - 90
tdchn1-50	06/18/95	68	100.5	0 - 100.5
tdchn2s [‡] -100	06/21/95	47	69 ft	279 -348
tdchn2s 50 MHz	06/21/95	45	66 ft	279 - 345

* omb & strob = oyster marker bed strike line

** strmsf = middle shoreface strike line

^f strtd = tidal delta strike line

^{ff} tdchn1 = tidal channel no. 1

[‡] tdchn2= tidal channel no. 2

Table 3 Common midpoint (3-fold) strike line

Line Name	Date	Number of Traces	Length (ft)	Starting & Ending Coordinates
tdcmp	06/22/95	74	438 ft	635 - 1073

2.0 PRELIMINARY EXAMINATION

There are basically two important portions to the GPR survey of outcrop G: (1) the 2D grid shot of the tidal delta sandstone at the top of the outcrop and (2) the multiple higher frequency surveys of the tidal channel in the lower part of the outcrop (Fig. 4).

The 2D grid of the tidal channel shot directly on the exposed sandstone surface provides the greatest opportunity to work with a signal unattenuated by surface clay. The multi-fold survey

is used to calculate the velocity or propagation of the radar through the tidal sandstones. Furthermore, because the survey over the tidal delta sandstone consists of one strike over the length of the exposure and two cross-cutting dip lines, there is the potential of examining the 3D bedding pattern within the tidal delta sandstone.

The 50 and 100 MHz coincident strike lines shot on top of the tidal channel sandstones could have provided the opportunity to image the accretionary surfaces with the channel sands. However, the local thin clay cover and the proximity of eroded edges of the sandstones have locally attenuated and interfered with the meaningful portions of the radar image and make interpretation difficult.

The degree to which these factors have affected the quality of the survey is evaluated first. Following this evaluation, the most meaningful portions of the GPR survey are subjected to further processing, interpretation, and analysis.

3.0 IMPROVING THE RADAR IMAGE

The quality of the data was strongly affected by the high water saturation of the outcrop. Groundwater perched within the outcropping sandstones was evidenced by the dampness of the base of outcrop core plugs and running water in the streams at the base of this and nearby outcrops. This meant that salts usually found on the surface of the soil were dissolved in the water within the sandstones. The consequences of this were twofold for the radar survey. First, this produced a strong reflection at the top of the sandstones that combined with the direct arrival to produce a strong event at the beginning of the signal and a markedly attenuated signal below (Fig. 5).

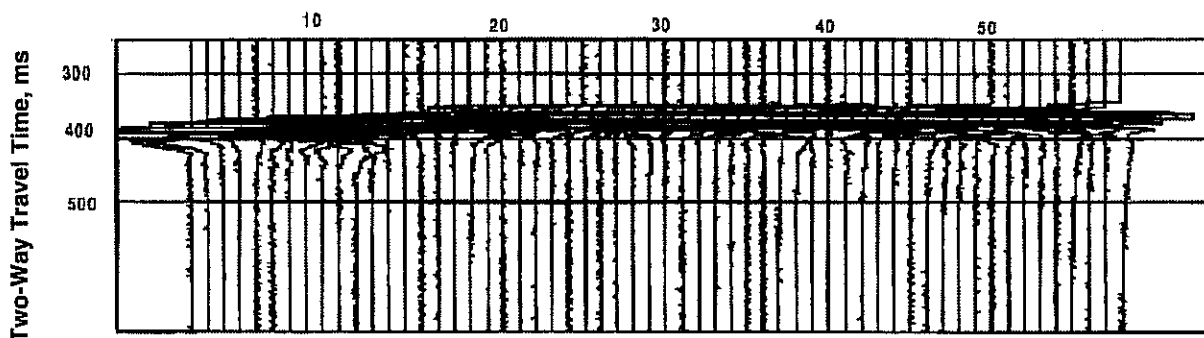


Figure 5 Dip line at 855 ft without any processing

Second, because of the conductivity of the sandstones, the direct current coupling between the receiving and transmitting antennae extended over a greater distance than is typical for outcropping sandstones (Fig. 6). Because of this, the spacing between the transmitter and receiver was twice the norm.

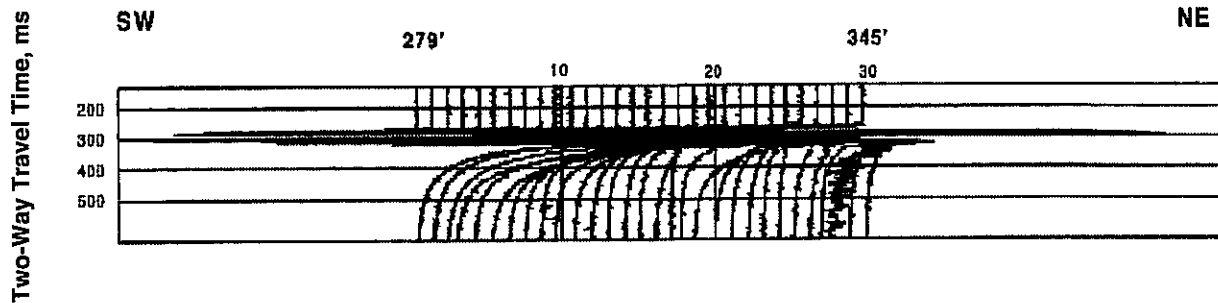


Figure 6 Distortion of signal due to DC coupling in line tdchn2s (MHz)

However, Figure 7 shows that this interference did not die away unless the two antennae were separated by 12 ft. Therefore only the tidal delta strike section composed from the third offset trace from each station of the common midpoint survey does not exhibit extreme distortion of the signal below the direct arrival.

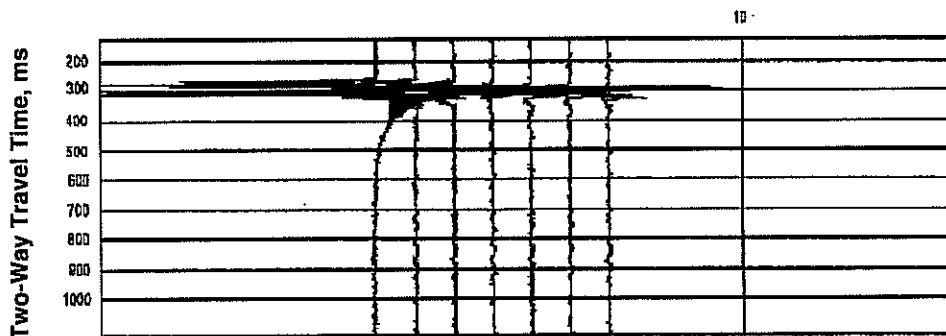


Figure 7 Shots of varying offset showing degree of DC coupling

To improve the resolution of the radar image, basic geophysical processing methods have been applied to the data including automatic gain control.

Static corrections were not necessary for the radar survey done over the tidal channel sands because there was no significant elevation difference between the transmitter and receiver or from station to station relative to the stratigraphic top of the tidal channel sands.

To enhance the low amplitude reflections without over-amplifying the strong reflections, automatic gain control (AGC) was applied to all the lines that were interpreted. The window of the AGC filter, 60 ns, was chosen to be slightly greater than that of the radar pulse wavelength. This choice produced the best images. A window more than one wavelength of the pulse would have smoothed the signal, and one of less would have enhanced the signal noise.

This process, while making stratigraphic interpretation possible, renders the resulting section useless for impedance inversion. Also, because of the quality of the GPR data, wavelet processing was not applied to any of the sections. It is not clear whether any preliminary processing could rectify this situation.

4.0 STRATIGRAPHIC INTERPRETATION

The methods of stratigraphic interpretation can be applied to this improved radar image. The geometric relationship of accretionary units within the sandstone bodies can be drawn.

The best lines for stratigraphic interpretation are the tidal delta common midpoint line, the portion of the dip line at 1075 ft, and the 100-MHz and 50-MHz oyster marker bed lines. Figure 4 shows a line constructed from the 18 ft offset traces from the tidal delta sandstone, common-midpoint survey. Several events can be seen below the direct and ground wave arrivals (approximately 250 ns). All of the events are discontinuous and generally do not extend beyond 120 ft.

The complete stratigraphic interpretation of this line is shown in Figure 8. Most of the events terminate against others, giving the section a large cross-bedded appearance (Fig. 9). The amplified signal becomes extremely noisy where it appears to enter under the underlying shale. The approximate base of the sandstone is drawn on the section where this noise starts in many traces.

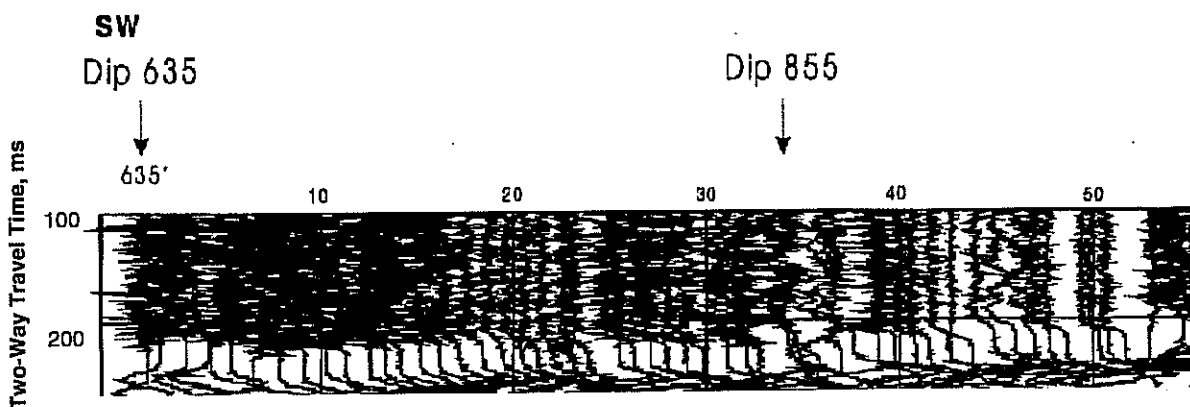


Figure 8 Tidal delta sandstone. Automatic gain control with a 60 ns window

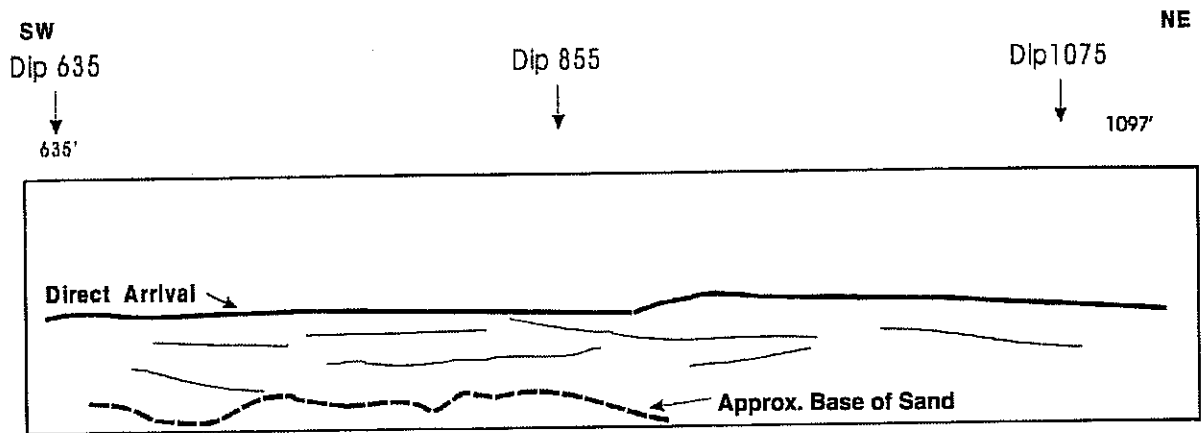


Figure 9 Stratigraphic interpretation of tidal delta GPR profile shown in Figure 8

The ability to draw cross-ties for stratigraphic events at intersections of GPR lines is important if 3D interpretations are to be attempted. The extension of dip line 1075 (Figs. 10 and 11) that runs nearly perpendicular to the tidal delta line of (Fig. 8) intersects the latter between traces 32 and 33. The same intersection on the tidal delta line is at trace 67. The same stratigraphic events can be seen in both sections 60 ns below the direct arrival.

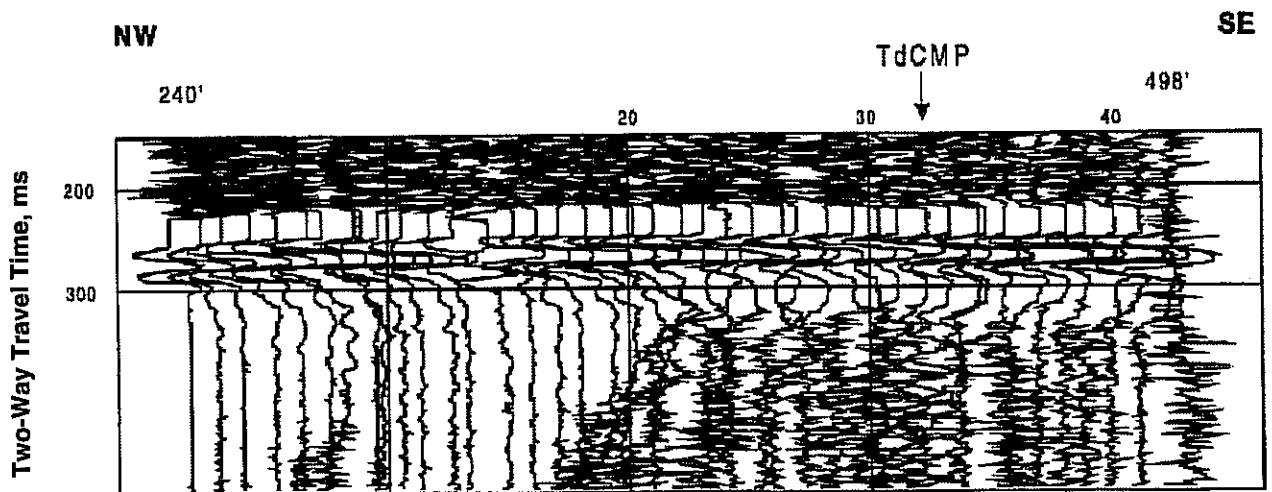


Figure 10 Dip line at 1075 ft with automatic gain control with a 60 ns window

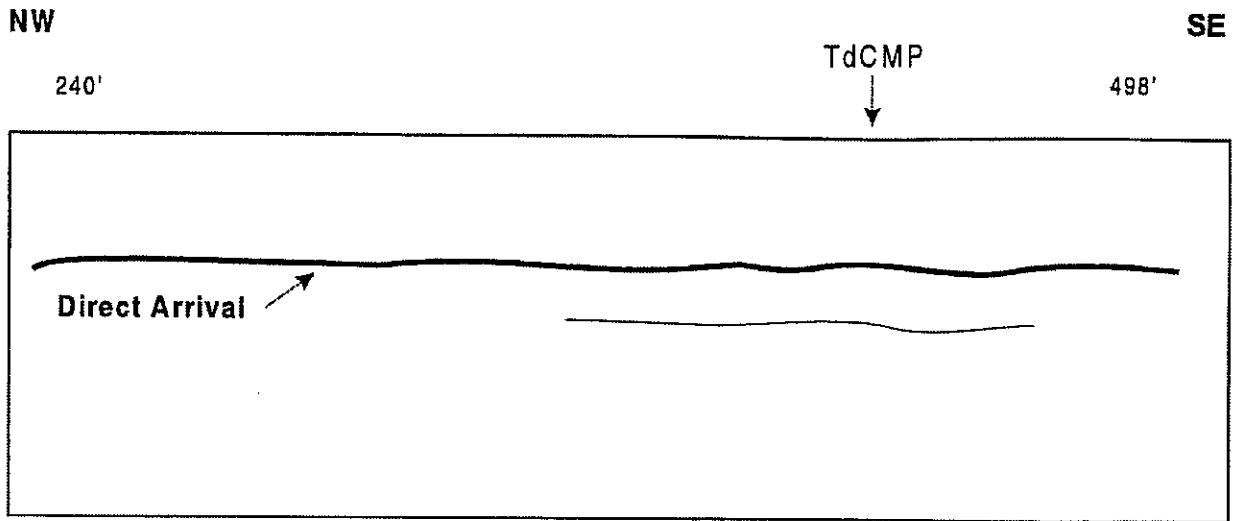


Figure 11 Stratigraphic interpretation of the tidal delta sandstone dip line 1075 ft shown in Figure 10

Two short lines of different signal frequency were shot over the oyster marker bed (Fig. 12). These two lines do not exhibit the problems seen in other lines. This is perhaps because these sandstones are more highly cemented, thus preventing ground water from saturating them and the underlying rocks. Both sections show the same lower frequency events in the lower half. These events appear to be the interbedded sandstones and shales of the lower part of the outcrop. Although the higher frequency (100 MHz) section appears to have more detail, much of this frequency variation is noise. In the case of the oyster marker bed near the top of the section, the events appear to be multiple reflections within the sandstone, not fine bedding.

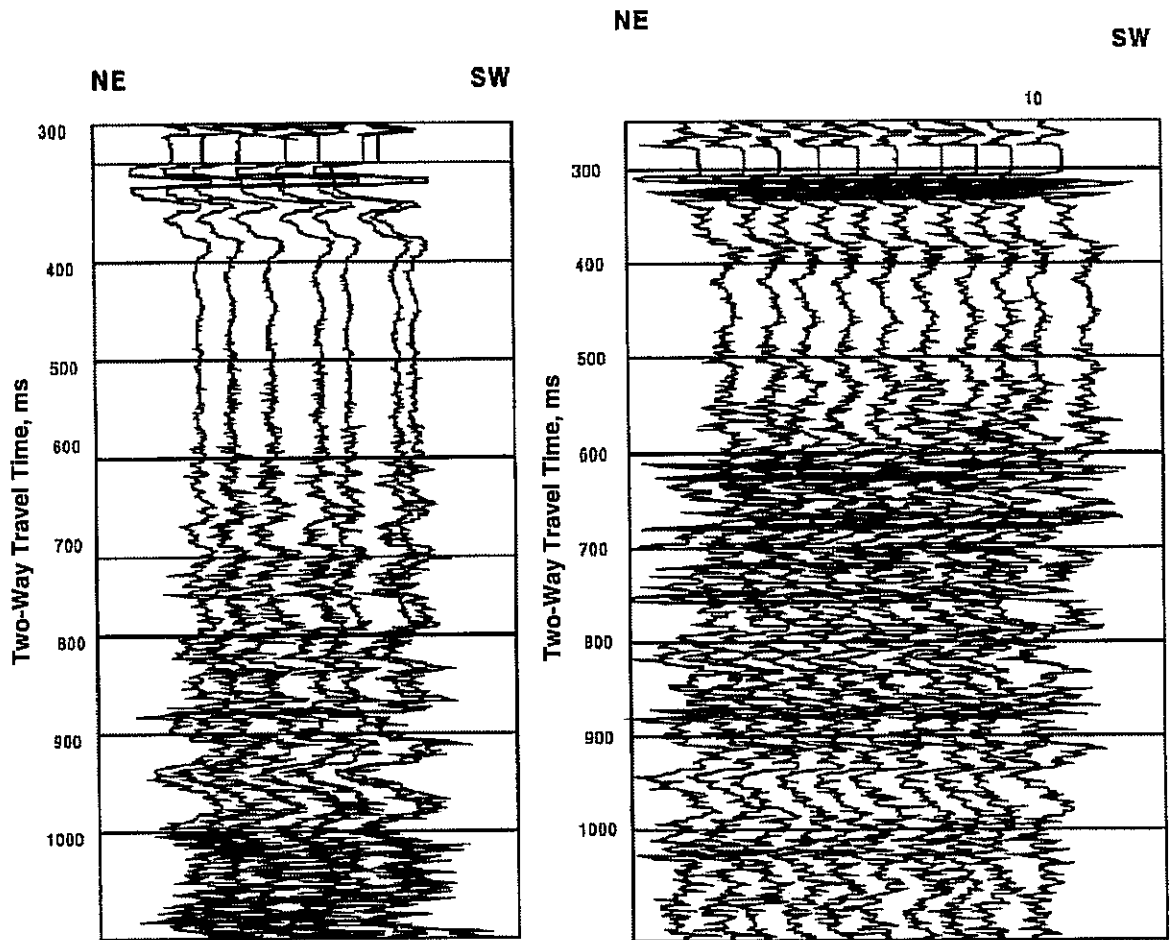


Figure 12 Strike line on oyster marker bed; 50 MHz (left) and 100 MHz (right)

The GPR section for Omb 50 appears to have several events below 700 ms. The tops of sandstones are indicated by positive events, and the tops of shales by negative events. The depth conversion for Omb 50 is based on the linear velocity estimation for sandstone. This velocity is probably too great for the underlying shale and coal. Therefore, the estimated depth to the underlying tidal channel and middle shoreface sandstones of approximately 84 ft is too great. The lower 300 ms from 700 to 1000 ms (Fig. 13) exhibit the alternating sandstone shale/coal bedding seen in the Almond formation core hole No. 2 (Schatzinger et al. 1993).

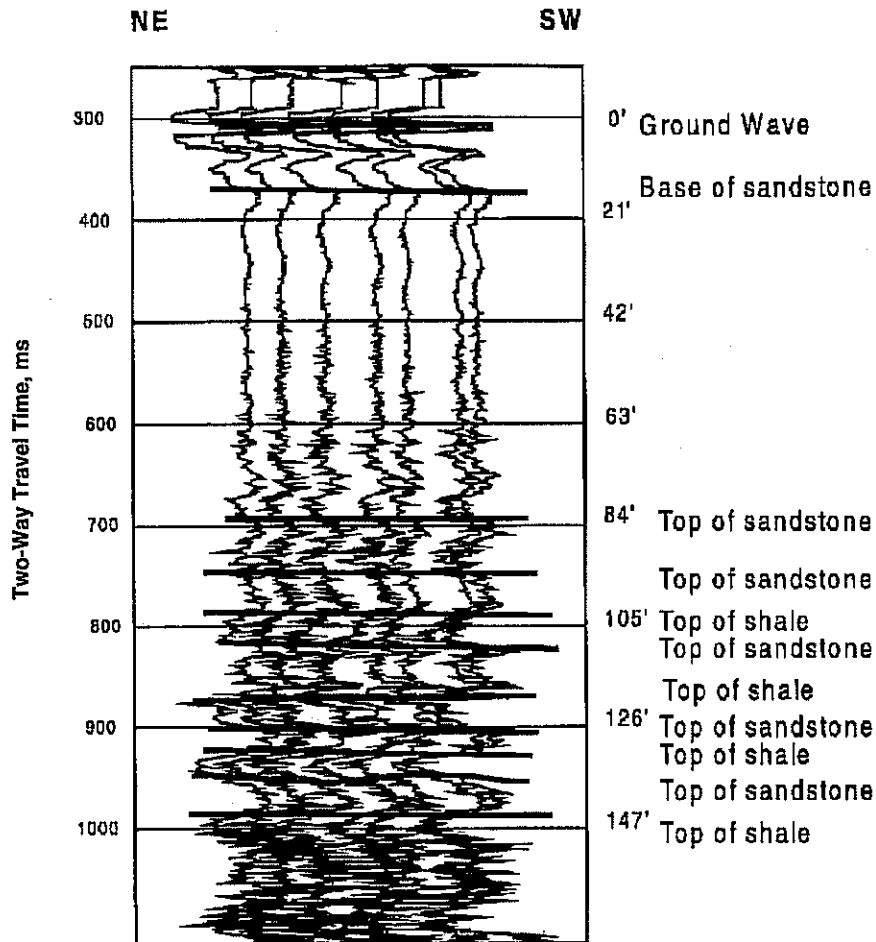


Figure 13 Stratigraphic interpretation of oyster marker bed line with estimated depth

5.0 VELOCITY ANALYSIS

Converting the radar image into a permeability image first requires a conversion of the radar interface image to a block property image. This block property image can then be converted to a permeability image through the correlation between spatially coincident core plug measurements and elements of the radar image.

The surfaces in the radar image can be related to the surfaces seen in the outcrop photographs. The travel time of events and distance between traces can be used to calculate the velocity of propagation of the radar through the sandstone.

The velocity of propagation through the tidal delta sandstone can be calculated using the time difference of the ground wave direct arrival among traces from different spacing of transmitter

and receiving antennae over a common midpoint. Figure 14 shows a line through the same event among the offset traces that has slope of 0.21 ft/ns (0.07m/ns). Considering this velocity, a 50 MHz wavelet with a wavelength of 20 ns can resolve beds about 1.5 ft thick, and the 100 Mhz wavelet can resolve beds thicker than 0.75 ft.

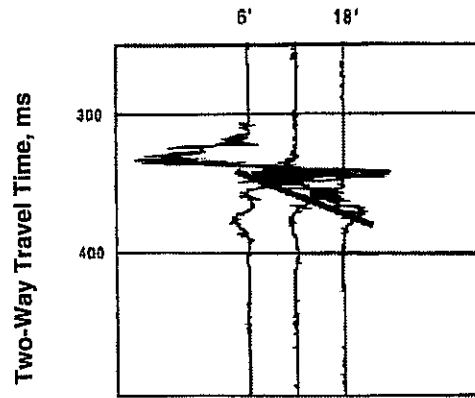


Figure 14 Velocity analysis of common midpoint traces centered on tdcmp line trace 72 for ground wave arrival

The velocity of the rock between reflecting layers can be used to calculate the impedance between layers which is related to electrical permittivity. Therefore, the radar image can be converted to an electrical permittivity image. Given a station separation of 1.5 ft, a sampling rate of 800 ps and a rock velocity of 0.21 ft/ns, a permittivity image could be made that would have 1.5×0.096 ft units.

However, because of the extreme attenuation of the signal by the water-saturated ground, the unprocessed traces have such a low signal-to-noise ration that a reliable impedance section cannot be developed. A more closely spaced grid of 2D lines acquired solely of the tidal delta sandstone at the top of the section would provide an excellent case for an impedance inversion. These impedance data could be used in conjunction with core permeabilities to generate a permeability image.

6.0 CONCLUSIONS

Bounding surfaces within strandplain/barrier island sandstones can be detected by 50 MHz or higher frequency GPR. With the velocity of propagation for the GPR in the sandstones of outcrop G now known to be about 21 ft per 100 ns, a survey could be designed for mapping the intrafacies accretionary units within these sandstones. A 100 MHz wavelet can resolve 0.75

beds, and a 200-MHz wavelet can resolve 0.375 ft beds. Wavelets of these wavelengths can be used to map the 1–4-ft-thick accretionary units of the tidal channel sandstones.

This survey has shown that 50 MHz signal was able to resolve beds thicker than about 1.5 ft found in the tidal delta sandstones. Therefore, a 2D widely spaced grid of GPR sections tied at their points of intersection or a closely and uniformly spaced grid can be used to generate a 3D image of the accretionary units within the tidal delta sandstones.

To ensure a GPR survey of the highest quality in a sequence of sandstones and shales such as the Almond formation at outcrop G, a preliminary electrical survey is essential to determine when conditions are suitable for the GPR survey. For further quality assurance, standard seismic interpretation software should be used during data acquisition so the survey design can be adjusted to suit the field conditions.

7.0 REFERENCES

- Aigner, T., U. Aspöck, J. Hornung, W.-D. Junghat, and R. Kostrewa. 1996. Integrated Outcrop Analogue Study of Triassic Alluvial Reservoirs: Examples from Southern Germany. *Journal of Petroleum Geology* v. 19: p. 393–406.
- Beres, M., Jr. and F. P. Haeni. 1991. Application of Ground-Penetrating-Radar Methods in Hydrogeologic Studies. *Ground Water* v. 29: p. 375–86.
- Chang, M. M., G. Guo, R. Schatzinger, and D. Lawson. 1994. *Geological and Engineering Techniques for Prediction Detection and Evaluation of Reservoir Bounding Surfaces*. DOE Report No. NIPER/BDM-0053, August.
- Jol, H. M., and D. G. Smith. 1991. Ground Penetrating Radar of Northern Lacustrine Deltas. *Canadian Journal of Earth Science* v. 28: p. 1939–47.
- Liner, C. L. and J. L. Liner. 1995. Ground-Penetrating Radar: A Near-Face Experience from Washington County, Arkansas. *The Leading Edge* January: p. 17–21.
- McMechan, G. A., R. B. Szerbiak, G. C. Gaynor, and C. J. Thompson. 1997. Use of Ground-Penetrating Radar for 3-D Sedimentological Characterization of Reservoir Analogs. *Geophysics* v. 62, no. 3: p. 786–796.
- Misra, D., M. Cil, R. A. Schatzinger, and J. Wheeler. 1997. *Modal and Geostatistical Analysis of Physical Properties: Almond Formation Transgressive Shoreline Barrier Facies, South-Central Wyoming*. DOE Report No. NIPER/BDM-0327, September.

- Olsen, H., and F. Andraesen. 1995. Sedimentology and Ground-Penetrating Radar Characteristics of a Pleistocene Sandur Deposit. *Sedimentary Geology* v. 99: p. 1–15.
- Press, W. H., S. A. Teukolsky, W. T. Vetterling, B. P. Flannery. 1992. *Numerical Recipes in C: The Art of Scientific Computing*. New York, N.Y.: Cambridge University Press, p. 994.
- Roehler, H. W. 1988. The Pintail Coal Bed and Barrier Bar G—A Model for Coal of Barrier Bar-Lagoon Origin, Upper Cretaceous Almond Formation, Rock Springs Coal Field, Wyoming. U.S. Geological Survey Prof. Paper 1398, p. 60.
- Schatzinger, R. A., and L. Tomutsa. 1997. Multiscale Heterogeneity Characterization of Tidal Channel, Tidal Delta and Foreshore Facies, Almond Formation Outcrops, Rock Springs Uplift, Wyoming. Fourth International Reservoir Characterization Technical Conference Proceedings, Houston, Texas, p. 199–217.
- Schatzinger, R. A., and J. Wheeler. 1997. Architectural Controls of Reservoir Quality in a Transgressive Barrier Shoreline: An Outcrop Study of the Almond Formation, Rock Springs Uplift, Wyoming. CSPG-SEPM Joint Convention, June 1–6, 1997, program with abstracts, p. 250.
- Schatzinger, R., M. Szpakiewicz, B. Sharma, and S. Jackson. 1993. *Petrophysical Characteristics Associated with Bounding Surfaces in Almond Formation Corehole No. 2, Sweetwater County, Wyoming*. DOE Report No. NIPER-720, December.
- Stephens, M. 1994. Architectural Element Analysis within the Kayenta Formation (Lower Jurassic) Using Ground-Probing Radar and Sedimentological Profiling, Southwestern Colorado. *Sedimentary Geology* v. 90: p. 179–211.
- Van Heteren, S., D. M. FitzGerald, P. A. McKinlay, and I. V. Buynevich. 1998. Radar Facies of Paraglacial Barrier Systems: Coastal New England, USA. *Sedimentology* v. 45: p. 181–200.
- Van Heteren, S., D. M. FitzGerald, D. C. Barber, J. T. Kelley, and D. F. Belknap. 1996. Volumetric Analysis of a New England Barrier System Using Ground-Penetrating-Radar and Coring Techniques. *Journal of Geology* v. 104: p. 471–483.

APPENDIX

This appendix contains GPR lines not discussed in the main text. Because of the DC coupling between antennae and the low signal to noise ration of these lines, both the consequence of high water saturation, it was not possible to make a stratigraphic interpretation of these lines. Events are visible in many of the sections, indicating the potential for stratigraphic interpretation under drier soil conditions.

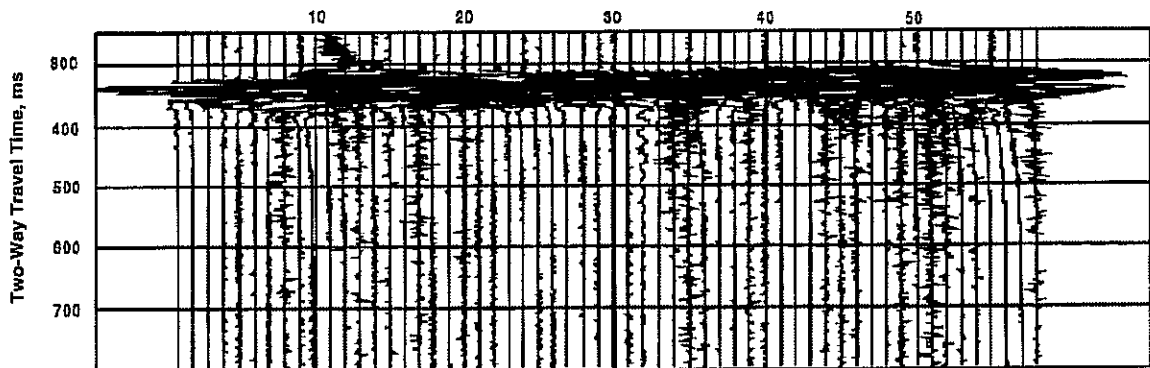


Figure A1 Dip line at 415 ft without any processing

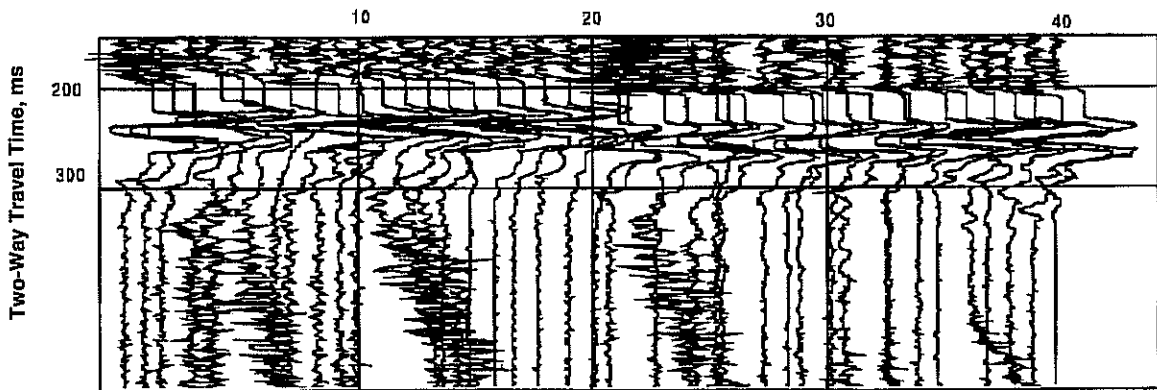


Figure A2 Dip line at 1075 ft. Automatic gain control applied with 60 ns window

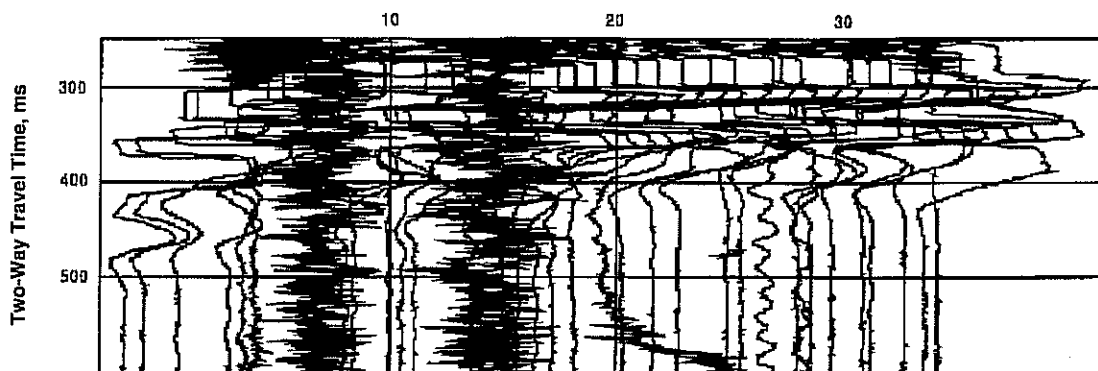


Figure A3 Strike line on oyster marker bed. Automatic gain control applied with 60 ns window

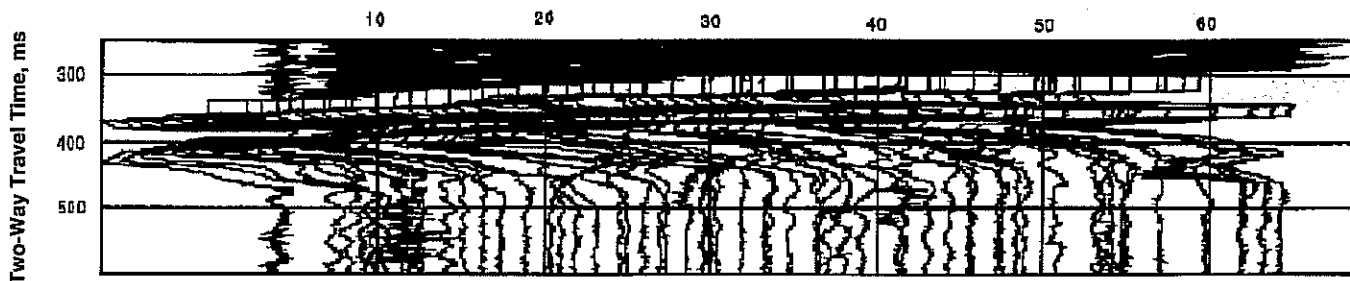


Figure A4 Middle shoreface strike line from 195 ft to 555 ft. Automatic gain control applied with 60 ns window

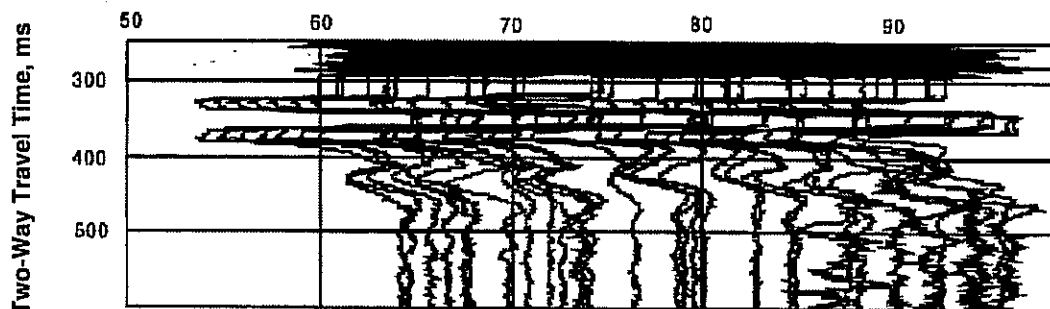


Figure A5 Continuation of middle shoreface strike line from 561 ft to 741 ft. Automatic gain control applied with 60 ns window

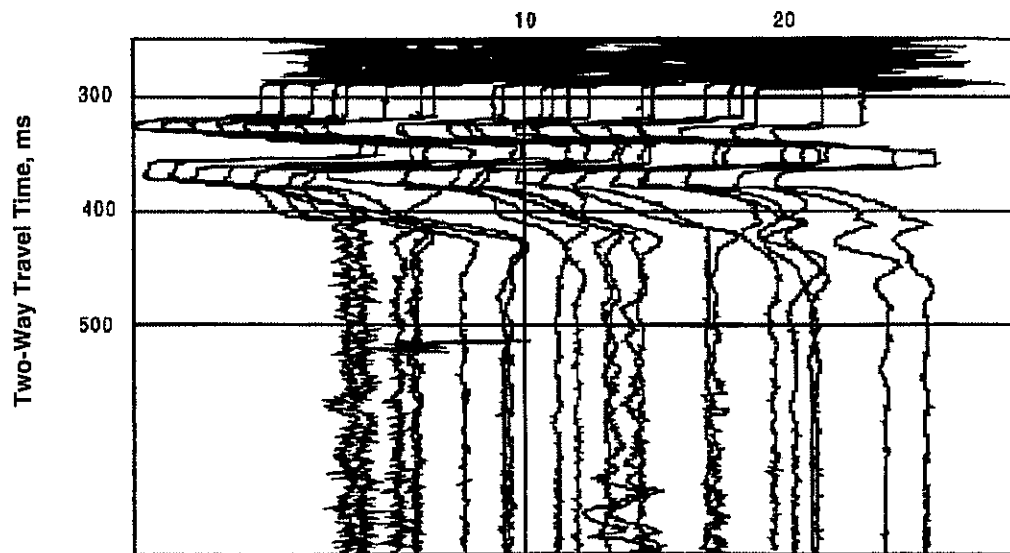


Figure A6 Middle shoreface strike line from 951 ft to 1077 ft. Automatic gain control applied with 60 ns window